dentistry journal

MDPI

Article

Enhanced Glass Ionomer Cement Restorations Using SHMP-Ag/Ti-ZSM-5 Zeolite Composite

Abdullah A. Aljami [1], Turki Alshehri [2], Fatimah M. Alatiyyah [3], Nizar Almousa [4], Rasha Alsheik [5], Suriya Rehman [6], Sarah Almofty [7] and Rabindran Jermy Balasamy [8,*]

1 Advanced Education in General Dentistry (AEGD), North of Riyadh Dental Center, Riyadh Second Health Cluster, Riyadh 13335, Saudi Arabia; draljama@gmail.com
2 Department of Substitutive Dental Science, College of Dentistry, Imam Abdulrahman Bin Faisal University, Dammam 31441, Saudi Arabia
3 Department of Genetics, Institute for Research and Medical Consultations (IRMC), Imam Abdulrahman Bin Faisal University, Dammam 31441, Saudi Arabia; fmalatiyyah@iau.edu.sa
4 College of Dentistry, Qassim University, Qassim 52571, Saudi Arabia; nizar.dent1@gmail.com
5 Department of Restorative Dental Science, College of Dentistry, Imam Abdulrahman Bin Faisal University, Dammam 31441, Saudi Arabia; ralsheikh@iau.edu.sa
6 Department of Epidemic Diseases Research, Institute for Research and Medical Consultations (IRMC), Imam Abdulrahman Bin Faisal University, Dammam 31441, Saudi Arabia; surrehman@iau.edu.sa
7 Department of Stem Cell Research, Institute for Research and Medical Consultations (IRMC), Imam Abdulrahman Bin Faisal University, Dammam 31441, Saudi Arabia
8 Department of Nanomedicine Research, Institute for Research and Medical Consultations (IRMC), Imam Abdulrahman Bin Faisal University, Dammam 31441, Saudi Arabia
* Correspondence: rjermy@iau.edu.sa

Abstract

Background: Glass ionomer cement (GIC) is widely used as a restorative and luting material, as it possesses cariostatic features that can manage coronal and root caries. However, GIC exhibits an initial burst release of fluoride during the setting reaction, followed by gradual decline with time, limiting its long-term anticariogenic properties. Previous studies have investigated the incorporation of chlorhexidine (CHX) with hexametaphosphate. **Objective**: This study aimed to prepare SHMP-functionalized silver-impregnated Ti-ZSM-5 zeolite as a potential SHMP carrier and to evaluate the effect of its incorporation into GIC on the surface roughness, color change, and antimicrobial properties. **Methods**: Titanium-incorporated ZSM-5 zeolite was acquired from Euro Support (Czechia). The 4 wt% Ag was impregnated on Ti-ZSM-5 (4 wt% Ag/Ti-ZSM-5) using the wet impregnation technique. The resulting silver-impregnated titanium zeolite composite was mixed with sodium hexametaphosphate (SHMP) using distilled water in a 1:1 ratio by grinding into a paste, which was followed by drying. The sample was characterized using X-ray diffraction analysis (XRD), N_2 adsorption–desorption, zeta potential, FT-IR, diffuse reflectance UV-visible (DRS UV-vis), scanning electron microscopy (SEM), energy-dispersive X-ray spectroscopy (EDX), elemental mapping and high-resolution transmission electron microscopy (TEM). Silver-impregnated titanium zeolite doped with SHMP samples was then mixed with GIC powder at ratios of 1%, 3%, and 5%, corresponding to ZSM-5@Ag/Ti 1%, ZSM-5@Ag/Ti 3%, and ZSM-5@Ag/Ti 5%. For comparison, Ag-silicalite was mixed with SHMP and GIC powder; the samples were designated as Z-Sil@Ag 1%, (F) Z-Sil@Ag 3%, and (G) Z-Sil@Ag 5% and tested for surface roughness, color change, cytotoxicity, and antimicrobial activity against *Streptomyces mutans* and *Candida albicans*. Statistical analyses were conducted using GraphPad Prism 11.1.0 and IBM SPSS Statistics 24. Normality was assessed using the Shapiro–Wilk and Brown–Forsythe tests, respectively. Group differences were evaluated using one-way and two-way ANOVA, which was followed by appropriate post hoc tests (Tukey's or Dunnett's) with effect sizes (ω^2), clinical acceptability thresholds ($\Delta E^* = 2.7$)

Check for updates

Academic Editor: Walter Dukić

Received: 1 September 2026
Revised: 4 November 2026
Accepted: 9 November 2026
Published: 15 November 2026

Copyright: © 2026 by the authors. Licensee MDPI, Basel, Switzerland. This article is an open access article distributed under the terms and conditions of the Creative Commons Attribution (CC BY) license.

and statistical significance set at $p < 0.05$. **Results**: The zeolite phase, metallic silver, and influence of SHMP deposition and GIC with 4 wt% Ag/TiZSM-5 particles was supported by XRD, BET, FT-IR, zeta potential, DRS-UV-vis, SEM-EDX and HR-TEM analysis. Surface roughness results showed that the ZSM-5@Ag/Ti group demonstrated comparable values to those of the control group, whereas Z-Sil@Ag–3% was the only group that differed significantly from the control ($p = 0.022$). The ZSM-5@Ag/Ti–5% group exhibited the lowest mean color change with all groups exceeding the clinical acceptability threshold ($\Delta E > 2.7$). All groups did not differ significantly in their antibacterial activity ($p > 0.05$) in comparison to the control. On one hand, the Z-Sil@Ag–5% group showed lower bacterial counts and thus higher antibacterial activity, whereas an adhesion test revealed that ZSM-5@Ag/Ti in all concentrations had the lowest counts. **Conclusions**: SHMP-functionalized 4 wt% Ag/TiZSM-5 could be incorporated into GIC without significantly altering its surface roughness with significant antimicrobial activity for dental applications.

Keywords: glass ionomer cement; cariostatic restoration; sodium hexametaphosphate; Ti-ZSM-5; silver nanoparticles; antimicrobial

1. Introduction

Cariostatic restoration materials, such as glass ionomer cements (GICs), have long been used for the management of coronal and root caries [1]. Their antibacterial effect has been reported to extend into neighboring tissues [1,2]. GICs have also attracted considerable research interest because of their ability to bond chemically to the tooth structure without requiring an additional bonding agent [2,3]. Nonetheless, GIC is capable of producing fluoride, and it goes through an initial burst of fluoride, especially during setting; then, it declines over time. However, studies have shown that GIC picks up fluoride from the oral cavity, but as the restoration ages, the ability diminishes over time [3,4]. Despite all the advantages GIC offers, there are still difficulties in determining its superiority in protection against caries. In a study by Hafshejani et al., they mentioned that fluoride release in GIC possibly stops after complete setting [5]. In addition, Loyola-Rodriguez et al. reported that complete bacterial eradication was not detected when GIC was used. Multiple studies used different antibacterial agents incorporated with GIC to enhance the antibacterial effect [3–6]. Current trends have involved incorporating silver particles to improve the antibacterial effect [7–9]. Nano-silver is implemented in dental fields such as endodontic applications [9], orthopedic implants [10], and glass ionomer cement [11]. Nano-silver particles affect bacterial cells through a variety of concurrent methods, such as the disruption and mechanical degradation of cell membranes and the modification of proteins in the intracellular medium [7,12,13]. Recent studies advocated for the use of nano-silver in combination with antibacterial monomers to enhance the antibacterial activity [10,11]. The antibacterial effect of silver in nano form has shown its efficacy in the prevention of secondary caries and multiple species of microorganisms such as *S. mutans*, *E. faecalis* and *S. aureus* [8,13].

Overall, the addition of materials to GIC has been shown to weaken its properties. One such material is sodium hexametaphosphate (SHMP). This material is known for its antibacterial effect and its ability to disintegrate dentinal inorganic material, which can occlude the dentinal tubules and thereby provide a desensitizing effect [12]. Several studies have also discussed the bleaching effect of SHMP when incorporated into restorative materials such as resins, which can accommodate active ingredients within their pores [13,14]. Mesoporous silica nanoparticles (MSNs) are among the materials capable of storing and release materials of choice in their porous matrix. Loading zinc (Zn) into

MSNs has been explored in dentistry [15]. For instance, Choi et al. used Zn-doped MSNs and bioactive glass to enhance remineralization and inhibit matrix metalloproteinases, resulting in higher bond strength [15,16]. MSNs are not limited to loading minerals and bioactive materials; they have also accommodate antibacterial agents like chlorhexidine (CHX). Incorporating CHX into MSNs resulted in sustained release within the dentinal tubules without compromising dentin bond strength [16]. Zeolites such as Zeolite Socony Mobil-5 (ZSM-5) have been exhaustively used in many applications as additives in petrochemical cracking processes, while silicalite has been used as an adsorbent in water filtration. A framework built with a Mobil Five (MFI) aluminosilicate structure contains micropores and exhibits excellent hydrothermal stability [17]. Silver–zeolite combinations have been reported to sustain silver ion release for up to 30 days and exhibit antibacterial activity in the oral cavity [18]. Incorporating heteroatoms such as titanium into the aluminosilicate framework (Ti-ZSM-5) may impart dental assistive property, while the impregnation of silver on Ti-ZSM-5 (Ag/Ti-ZSM-5) may boost the antibacterial activity. This material may therefore have potential for improving the antimicrobial and physical properties of restorative materials. The issue associated with SHMP in the literature is that it liquifies the matrix of the involved restoration, which hinders its properties and setting time in GIC. Hexametaphosphate-based agents have previously been incorporated into GIC mainly as chlorhexidine–hexametaphosphate particles [9,14], and silver-based additives have been investigated to enhance the antibacterial properties of GIC [13]. However, to the best of our knowledge, Ag/Ti-ZSM-5 zeolite has not previously been investigated as a carrier for SHMP in GIC. Therefore, this proof-of-concept in vitro study aimed to prepare an SHMP-functionalized Ag/Ti-ZSM-5 micron-sized zeolite composite and evaluate the effects of its incorporation into GIC on the surface roughness, color change, antibacterial activity against *S. mutans*, and *C. albicans* adhesion.

2. Materials and Methods

2.1. Sample Calculation and Study Groups

The sample size for the current study was calculated based on the results of a previous study [14]. G*power 3.1.9.4 software was used for calculation. The predicted sample for each group was a total of ($n = 5$) samples, using 0.05 as the level of significance and 0.92 as the effect size, and power was kept at 95%.

The study groups were divided as shown in Table 1.

Table 1. Study groups.

No.	Group Composition	Addition	Concentration
1	GIC	No addition	-
2	GIC with ZSM-5@	Ag/Ti	1%
3			3%
4			5%
5	GIC with Z-Sil@	Ag	1%
6			3%
7			5%

2.2. Samples Preparation

2.2.1. Silver Impregnated on TiZSM-5 (4 wt% Ag/Ti-ZSM-5)

Fifty grams of TiZSM-5 zeolite particles were acquired from Euro support (Czechia). First, 0.126 g of silver nitrate was dissolved in 60 mL of water; then, we added 2 g of Ti-ZSM-

5, stirred overnight, and dried at 100 °C for 6 h. The sample was then calcined at 550 °C for 3 h. The sample was designated as ZSM-5@Ag/Ti.

2.2.2. Ag-Silicalite (Z-Sil@Ag)

Ag-incorporated silicalite-1 (Z-Sil@Ag) was synthesized via a hydrothermal method. Briefly, 0.93 g of sodium hydroxide (NaOH) was dissolved in 9 mL of deionized water under magnetic stirring for 5 min until complete dissolution. Subsequently, 11.42 g of Ludox AS-40 colloidal silica was added dropwise. A solution containing 0.52 g of silver nitrate was then added to the reaction mixture under continuous stirring. Subsequently, 8.0 g of tetrapropylammonium hydroxide (TPAOH, 40 wt%) was introduced dropwise, and the resulting precursor gel was stirred overnight. The homogeneous gel was then aged 24 h before being transferred into a 250 mL Teflon-lined stainless-steel autoclave for hydrothermal crystallization at 160 °C for 72 h under static conditions. After crystallization, the solid product was recovered by filtration, thoroughly washed, and dried overnight. The dried sample was subsequently calcined at 550 °C for 6 h with a heating rate of 5 °C min^{-1}. The final product was designated as Z-Sil@Ag.

2.2.3. Synthesis of 4 wt% Ag/Ti-ZSM-5/SHMP or Z-Sil@Ag/SHMP Composite

The 4 wt% Ag/Ti-ZSM-5/SHMP composite was prepared using the incipient wetness impregnation method. Briefly, 1.0 g of sodium hexametaphosphate (SHMP) and 1.0 g of 4 wt% Ag/Ti-ZSM-5 were accurately weighed and mixed in a 1:1 (w/w) ratio using a mortar and pestle. Distilled water was added dropwise while continuously grinding the mixture for 10 min until a homogeneous thick paste was obtained. The paste was subsequently dried in a hot-air oven at 60 °C overnight to remove excess moisture. The dried material was then gently ground into a fine powder using a mortar and pestle and stored in airtight containers for subsequent characterization and incorporation into GIC. A similar procedure was followed to prepare the Z-Sil@Ag/SHMP composite.

2.2.4. Synthesis of 4 wt% Ag/Ti-ZSM-5/SHMP-Modified Glass Ionomer Cement (ZSM-5@Ag/Ti–1%, ZSM-5@Ag/Ti–3%, and ZSM-5@Ag/Ti–5%)

GIC composites containing 4 wt% Ag/Ti-ZSM-5/SHMP composite were prepared by a dry-mixing technique. Briefly, 5.0 g of commercial luting cement glass ionomer cement powder (Securafix Glass Ionomer Luting Cement, Willmann & Pein Dental, Hamburg, Germany) was mixed with predetermined amounts of the 4 wt% Ag/Ti-ZSM-5/SHMP composite using a mortar and pestle until a homogeneous powder was obtained. The composite was incorporated at concentrations of 1 wt% (0.05 g), 3 wt% (0.15 g), and 5 wt% (0.25 g) relative to the GIC powder. The resulting formulations were designated as ZSM-5@Ag/Ti–1%, ZSM-5@Ag/Ti–3%, and ZSM-5@Ag/Ti–5%, respectively. A conventional luting GIC was used as the base material in this proof-of-concept study; therefore, the findings should be confirmed in restorative-grade GIC formulations before being extrapolated to restorative applications.

2.2.5. SHMP Delivery

The release study of SHMP from the 4 wt% Ag/TiZSM-5/SHMP composite was studied using the dialysis membrane method at 37 °C. Briefly, 15 mg of sample was included inside the pre-activated dialysis membrane and immersed in buffer solutions maintained at pH 7.4. At specific time periods, 5 mL of the release medium was withdrawn, replaced with fresh solution and analyzed for SHMP content by UV-visible spectroscopy.

2.2.6. GIC Discs Preparation

Disc-shaped samples (10 mm in diameter and 2 mm in thickness) of GIC were prepared as shown in Figure 1. Each sample was mixed using a plastic spatula on a mixing-pad following the manufacturer's instructions. A single operator performed the mixing step for all samples using 2 drops of liquid and 1 level measuring scoop of powder, and the powder contained calcium aluminum fluorosilicate in ~75%, polyacrylic acid in ~25%, liquid with tartaric acid in >6% and water in >90%. It was mixed until a homogenous mixing was ensured. Then, we applied it into a mold which was covered with clear polyester strips and glass slides [19]. The sample edges were polished with sandpaper after 24 h. The samples were tested for surface roughness and color change; then, we measured for antimicrobial efficacy.

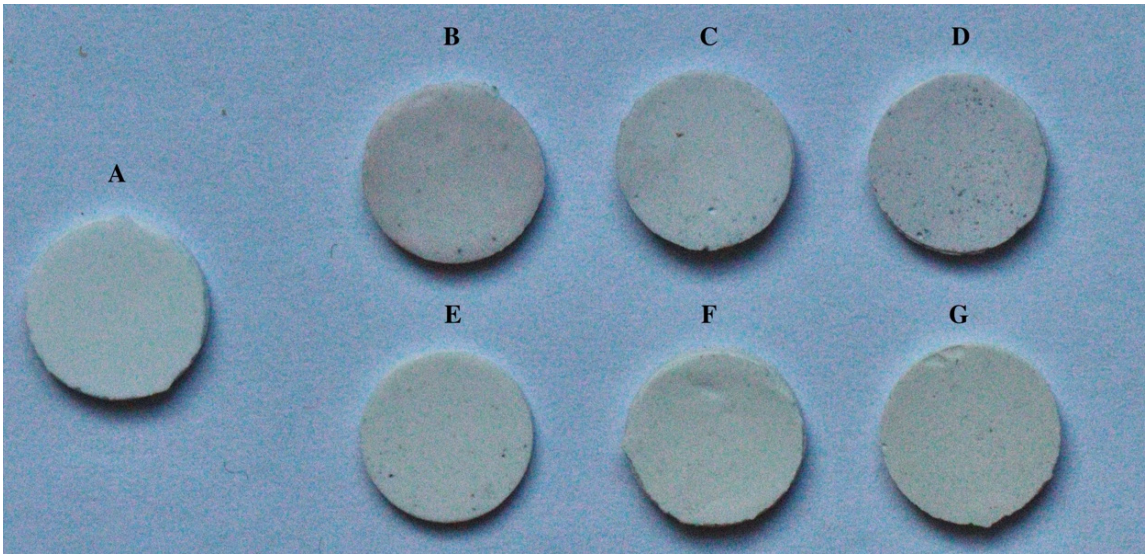


Figure 1. Photographs of GIC discs. (**A**) GIC control, (**B**) ZSM-5@Ag/Ti 1%, (**C**) ZSM-5@Ag/Ti 3%, (**D**) ZSM-5@Ag/Ti 5%, (**E**) Z-Sil@Ag 1%, (**F**) Z-Sil@Ag 3%, (**G**) Z-Sil@Ag 5%.

2.3. Characterization and Study Assessments

2.3.1. Physicochemical Analysis

After collecting functionalized titanium ZSM-5 zeolite particles with SHMP, samples were prepared for scanning electron microscopy to assess the SHMP salt surface coverage on the zeolite particles, and EDX elemental mapping was used to detect the presence of SiO_2, silver, and titanium inside the composite. The morphology texture of the Ag/Ti-ZSM-5 and Ag/Ti-ZSM-5/SHMP/GIC composites was analyzed using high-resolution transmission electron microscopy (JEM2100F from JEOL Ltd., Tokyo, Japan). The external texture of the composites was analyzed using SEM-EDS (JSM-6610LV, JEOL Ltd., Japan), while elemental mapping was obtained by energy-dispersive spectroscopy (EDS) using Aztec software (Oxford Instruments, High Wycombe, UK). The zeolite phase of TiZSM-5 and Ag-impregnated TiZSM-5 were analyzed using benchtop XRD (Miniflex 600, Rigaku Co., Tokyo, Japan). Titanium, silver, SHMP, and GIC coordination through absorption versus wavelength (nm) was measured using solid sample analysis and diffuse reflectance UV-visible spectroscopy (JASCO, Tokyo, Japan). The interaction of silver and TiZSM-5 was confirmed using Fourier transform infrared (FT-IR) spectroscopy (L160001J, Perkin Elmer, Waltham, MA, USA). The zeta potential of the five samples was identified using the Zetasizer NanoZS (Malvern, UK).

2.3.2. Surface Roughness (Ra) and Color Change Measurements

The surface roughness of the GIC-modified Z-Sil@Ag and ZSM-5@Ag-Ti at 1, 3, and 5% was measured using a non-contact optical profilometer (Contour Gt-K 3D optical profiler, Bruker Nano GmbH, Berlin, Germany). Three readings were detected for each sample with each composite having ($n = 5$) on different regions at a speed of 0.5 mm per second; the cutoff was set to 0.8 mm, and the mean of the Ra readings was calculated [19].

The color change was assessed using a reflectance spectrophotometer (Color-Eye 7000A; X-Rite, Grand Rapids, MI, USA). The Commission Internationale de l'Eclairage (CIE) L*a*b*color scale was used to measure the color as the L*a*b* system represents a three-dimensional color space: L* represents lightness from black to white from zero to 100, while a* and b* represent chromaticity with no specific numeric limits. Negative a* corresponds with green, positive a* corresponds with red, negative b* corresponds with blue, and positive b* corresponds with yellow. The color of each sample was calculated using the following formula [19]:

$$\Delta E^* = [(\Delta L^*)2 + (\Delta a^*)2 + (\Delta b^*)2]1/2$$

2.3.3. Antibacterial Efficacy

The antimicrobial activity of GIC-modified Z-Sil@Ag and ZSM-5@Ag-Ti at 1, 3, and 5% was evaluated against *Streptococcus mutans* (ATCC 25175). *S. mutans* were cultured overnight in Brain–Heart Infusion (BHI) broth at 37 °C for 24 h. Prior to microbiological testing, the samples were individually placed into sterile 24-well plates and sterilized by ultraviolet (UV) irradiation for 30 min.

Each sterilized specimen was transferred to an individual well of a sterile 24-well plate containing 1 mL of BHI broth supplemented with sucrose to promote biofilm formation. Subsequently, 50 µL of the standardized *S. mutans* suspension was inoculated into each well. The plates were incubated at 37 °C for 24 h under 5% CO_2 to allow bacterial adhesion and biofilm formation. Following incubation, each specimen was gently rinsed with sterile phosphate-buffered saline (PBS) to remove non-adherent bacterial cells. The adherent biofilm was recovered by transferring each specimen into a sterile tube containing 1 mL of PBS, which was followed by vortex mixing for 30 s and ultrasonic treatment for 10 min to detach the biofilm from the specimen surface. The recovered biofilm suspension was serially diluted in sterile PBS to obtain a ten-fold dilution. From each dilution, 100 µL was spread onto BHI agar plates. The agar plates were incubated at 37 °C for 48 h under 5% CO_2. After incubation, colonies were manually counted, and bacterial counts were corrected using the corresponding dilution factor. The results were expressed as $\log_{10}$ colony-forming units per milliliter ($\log_{10}$ CFU/mL) [20].

2.3.4. Microbial Adhesion Test

Preparation of Inoculum:

Candida albicans (ATCC 14053) was selected to examine the surface adhesion on the synthesized discs. An inoculum of *C. albicans* was prepared in Sabouraud dextrose broth (SDB) at 37 °C and incubated with shaking conditions for 48 h. Post incubation, Candida cells were obtained by centrifugation and adjusted to a final concentration of 3×10^3 CFU/mL in phosphate saline buffer (PBS) by spectrophotometry.

Adhesion Test:

The standardized fungal culture suspension (1 × 106 CFU/mL) in SDB was used to submerge the GIC disc. Subsequently, the discs were incubated at 37 °C overnight under static conditions to allow for the initial adhesion and biofilm formation of Candida. Further, after the 24 h incubation period, the culture medium was removed and replaced with fresh SDB to submerge the discs; then, it was incubated under the same conditions. Post

incubation, the discs were gently transferred in 9. 95 mL PBS (pH 7.5). Later, the disc samples were vortexed to detach the adherent Candida cells from the surface to obtain a uniform cell suspension. The suspension was serially diluted, and further selected dilution was spread on the freshly prepared SDA plates. The plates were further incubated at 37 °C for 48 h. On completion of incubation, the number of colony-forming units (CFUs) was calculated and expressed as CFU per disc. The rate of adhesion of the Candida was determined by the following formula: Adhesion % = (A/B) × 100 (where A is the number of CFUs in the prepared discs, and B is the number of CFUs in the control disc).

2.3.5. In Vitro Cytotoxicity

The human foreskin fibroblast HFF-1 (ATCC SCR-C-1041™, Manassas, VA, USA) cells were used to evaluate cytotoxic activity and were cultured in Dulbecco's Modified Eagle Medium (DMEM) supplemented with 10% heat-inactivated fetal bovine serum (HI-FBS), 1% penicillin–streptomycin (P/S), 1% non-essential amino acids (MEM-NEAA), and 1% L-glutamine. All reagents were sourced from Thermo Fisher Scientific (Waltham, MA, USA). Cells were plated in sterile 96-well flat-bottom plates at 10^4 cells per well in 100 µL of medium. After 24 h of incubation to allow attachment, composites (4 wt% Ag/Ti-ZSM-5, 4 wt% Ag/Ti-ZSM-5/SHMP, 1% of (4 wt% Ag/Ti-ZSM-5/SHMP)-GIC, Ti-ZSM-5 alone, and GIC) were serially diluted in DMEM to produce six concentrations (1–6): 6.25, 12.5, 25, 50, 100, and 200 µg/mL. Additional serial dilutions of $AgNO_3$ were prepared based on its ratio (6.3%) in each composite, ranging from 0.4 to 12.6 µg/mL.

The MTT assay (M2128, Sigma-Aldrich, St. Louis, MO, USA) assessed the composites' cytotoxicity by measuring MTT reduction to formazan, which is an indicator of viable, metabolically active cells. After 48 h of treatment, 20 µL of MTT solution (5 mg/mL in PBS) was added to each well; then, they were incubated in the dark at 37 °C for 4 h. The supernatant was then carefully removed, and 100 µL of DMSO was added to dissolve the formazan crystals. Absorbance was measured at 570 nm with a Synergy Neo2 microplate reader (BioTek Instruments, Winooski, VT, USA). Data from cells treated with composites (Sample) were compared with those from untreated cells (NTC), which served as the 100% cell-growth control. All conditions were tested in triplicate to ensure reproducibility.

The cell viability (%) was calculated as follows:

$$\text{Cell Viability (\%)} = (\text{Sample Abs})/(\text{NTC Abs}) \times 100$$

2.4. Statistical Analysis

Statistical analyses were performed using GraphPad Prism software version [11.1.0] for [macOS] (GraphPad Software, La Jolla, CA, USA). Data are presented as the mean ± SD with 95% confidence intervals ($n = 5$ samples per group). The normality of ANOVA residuals was assessed with the Shapiro–Wilk test, and the homogeneity of variances was assessed with the Brown–Forsythe test. For the distribution assumption, a Gaussian normal distribution was assumed. For surface roughness. Ra values (µm) of the control and six studied groups were compared using ordinary one-way ANOVA followed by Tukey's multiple comparisons test. For color change, ΔE* was calculated for each sample relative to the control's mean L*, a*, and b*, using the CIELAB formula $\Delta E^* = [(\Delta L^*)^2 + (\Delta a^*)^2 + (\Delta b^*)^2]1/2$. The six studied groups were compared using ordinary one-way ANOVA followed by Tukey's multiple comparisons test. The clinical relevance was defined as a 50:50% acceptability threshold ($\Delta E^* = 2.7$) using a one-sample *t*-test [21]. For antibacterial efficacy, viable *Streptococcus mutans* values of Log_{10} (CFU/mL) were compared using one-way ANOVA followed by Dunnett's multiple comparisons test against the control.

The effect size was calculated for each one-way ANOVA test as ω^2 = (SS_between-df_between × MS_within)/(SS_total + MS_within) with 95% CIs. This measure was chosen because it is less biased than eta squared for small samples [22]. Data for the MTT assay are presented as the mean ± standard deviation (SD) from two independent experiments. The statistical significance between groups was assessed using repeated-measures two-way ANOVA with Geisser–Greenhouse correction, which was followed by Tukey's multiple-comparisons test. A p-value < 0.05 was considered statistically significant. Multiplicity-adjusted p-values are reported for all post hoc comparisons. All other statistical analyses were performed using IBM SPSS Statistics version 24 (IBM Corp., Armonk, NY, USA).

3. Results

3.1. X-Ray Diffraction Analysis (XRD)

X-ray diffraction (XRD) analysis was performed to investigate the crystalline phases of pristine TiZSM-5 and 4 wt% Ag/TiZSM-5 integrated with SHMP (Figures 2 and 3a,b). TiZSM-5 exhibited reflections characteristic of the MFI zeolite framework. After silver loading, these reflections were retained, indicating the intactness of crystalline framework throughout the modification process. However, the Ag-loaded sample exhibited a slight reduction in diffraction peak intensity compared with pristine TiZSM-5. This reduction may be associated with the deposition of Ag nanoparticles and SHMP surface coverage, which partially covered the zeolite crystallites and slightly reduced the overall crystallinity. This decrease in peak intensity may be related to the deposition of silver species, which may partially cover the zeolite crystallites and slightly reduce the X-ray scattering intensity [23]. Weak but distinct peaks corresponding to (111) and (200) planes of metallic silver were also observed, indicating the presence of crystalline Ag domains associated with the TiZSM-5 particles. Nitrogen adsorption–desorption measurements were performed to evaluate the textural properties and accessible porosity of TiZSM-5 and 4 wt% Ag/TiZSM-5 (Figure 3c,d). Pristine TiZSM-5 exhibited a BET surface area of 330 m^2/g, a micropore surface area of 161 m^2/g, a total pore volume of 0.29 cm^3/g, and an average pore diameter of 3.5 nm. Following Ag impregnation, the BET and micropore surface areas decreased to 267 and 131 m^2/g, respectively, while the total pore volume decreased to 0.26 cm^3/g. These reductions are consistent with the occupation or partial blockage of pores and pore entrances by silver species, reducing nitrogen accessibility, as previously reported for Ag-modified ZSM-5 [24]. The external deposition around the pores slightly increased to 4.0 nm (Figure 3c,d). The FTIR spectra of TiZSM-5 and Ag-impregnated TiZSM-5 are presented in Figure 3e,f. TiZSM-5 exhibited a characteristic band at approximately 543 cm^{-1}, which was attributed to double five-membered ring vibrations of the MFI zeolite framework [25]. Following Ag impregnation, this band remained detectable but exhibited decreased in intensity, suggesting preservation of the framework with changes in its vibrational response. A more pronounced decrease was observed in the broad O–H stretching region, particularly at approximately 3000–3700 cm^{-1} within the examined range of 2500–4000 cm^{-1}. This decrease is consistent with the involvement of surface hydroxyl groups in anchoring silver species, as reported for Ag-modified ZSM-5 [26]. The surface charge and colloidal stability of TiZSM-5, 4Ag/TiZSM-5, 4Ag/TiZSM-5/SHMP, and the corresponding GIC composites containing 3% and 5% additive were assessed using zeta-potential measurements. Dispersion stability is relevant to minimizing additive aggregation during dental composite preparation. Following SHMP modification, the zeta potential reached −42.90 mV, indicating a strongly negative surface potential and suggesting favorable electrostatic stabilization under the measurement conditions. This behavior may be attributed to the adsorption of anionic phosphate groups from SHMP onto the particle surface, thereby increasing interparticle repulsion. A similar mechanism has been reported for SHMP-modified inor-

ganic particles, in which an increased negative surface charge reduced aggregation and improved dispersion [27]. These findings suggest that SHMP functionalization promotes the dispersibility of Ag/TiZSM-5 for incorporation into GIC.

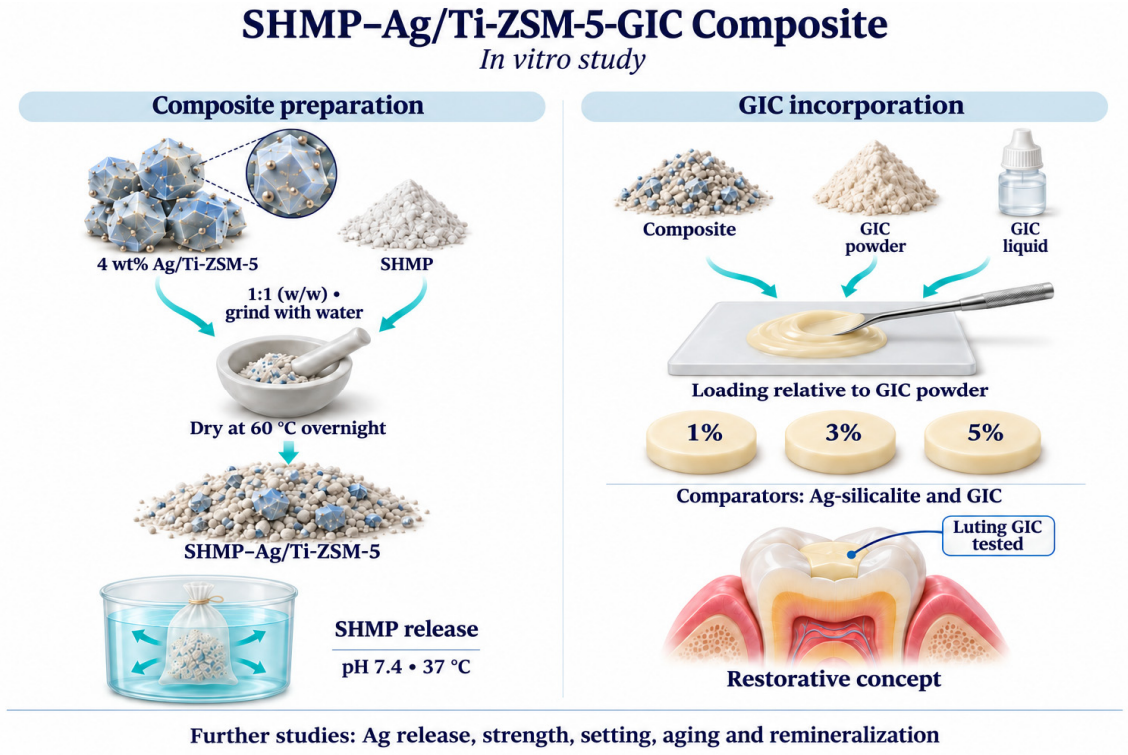


Figure 2. Schematic representation of Ag/TiZSM-5/SHMP/GIC (ZSM-5@Ag/Ti) formulation.

3.2. Scanning Electron Microscopy and Energy-Dispersive X-Ray Spectroscopy Analysis (SEM/EDX)

Scanning electron microscopy (SEM) was performed to investigate the surface morphology of the 4 wt% Ag/TiZSM-5 and 4 wt% Ag/TiZSM-5 /SHMP (Figure 4a–k). Figure 4a,b present the SEM micrograph and energy-dispersive X-ray spectroscopy (EDX) analysis of 4 wt% Ag/Ti-ZSM-5, respectively. The SEM image reveals agglomerated, micrometer-sized particles with irregular shapes and rough surfaces. EDX analysis identifies O, Si, Al, Ti, and Ag, which is consistent with the composition of the silver-loaded, Ti-containing zeolite. The measured Ag content of 3.49 wt% supports successful silver impregnation and is reasonably close to the nominal loading of 4 wt%, considering the localized, semiquantitative nature of EDX analysis. The SEM image of 4 wt% Ag/TiZSM-5/SHMP shows agglomerated particles forming irregular clusters with rough, heterogeneous surfaces (Figure 4c). The corresponding EDX spectrum of 4 wt% Ag/TiZSM-5/SHMP shows predominantly Si and O, together with the Ti, Al, and Ag signals, supporting the presence of impregnated silver on TiZSM-5 (Figure 4d). The SEM-EDX micrographs showed deposits consistent with sodium hexametaphosphate (SHMP) on the surface of the Ag/TiZSM-5 zeolite particles without any apparent alteration of the overall morphology of the zeolite crystals (Figure 4e–k). Furthermore, the elemental mapping revealed the presence and spatial distribution of Na and P (Figure 4i,j), which is consistent with SHMP deposition on the Ag/TiZSM-5 particles.

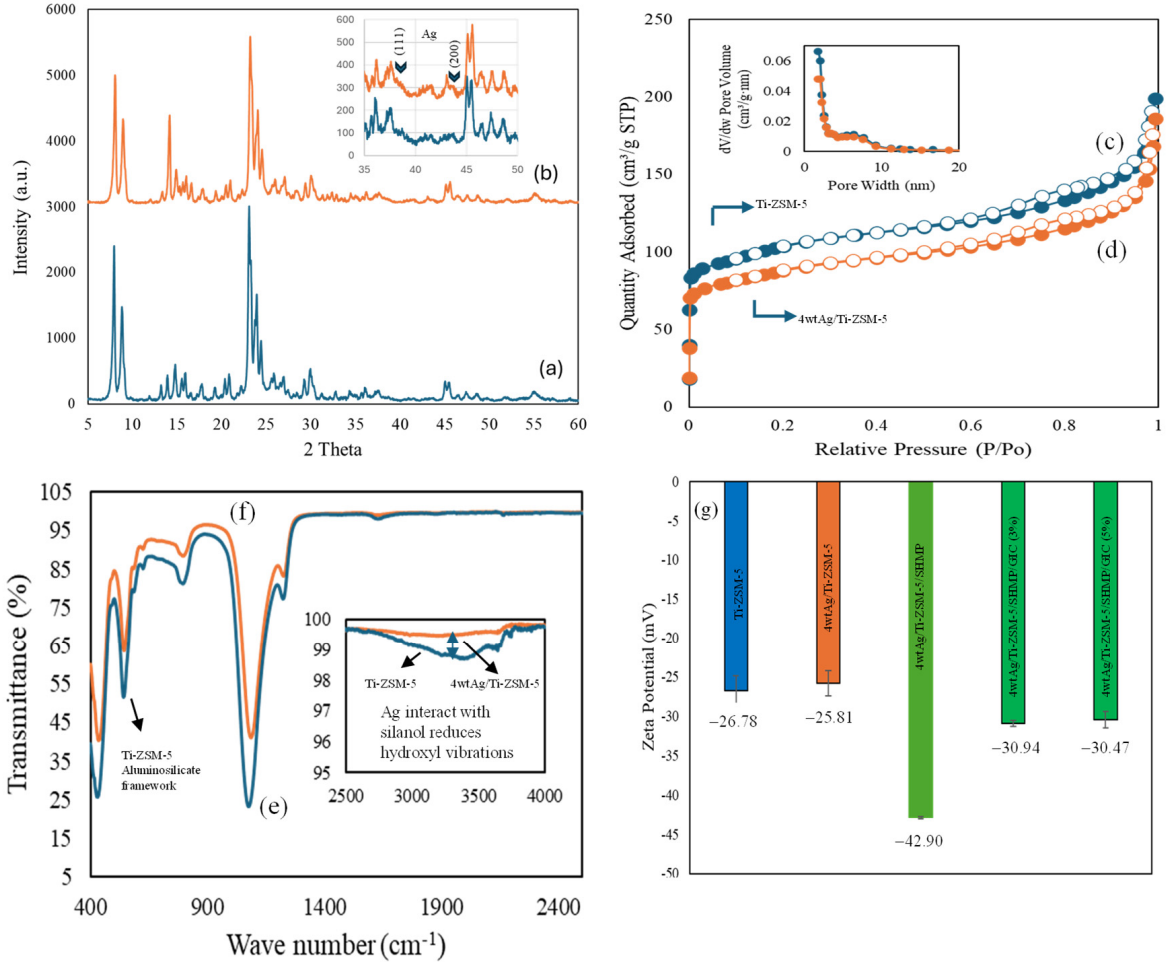


Figure 3. Physicochemical characterization of TiZSM-5 and its composites: X-ray diffraction (XRD) patterns of (**a**) TiZSM-5 and (**b**) 4 wt% Ag/TiZSM-5; nitrogen adsorption–desorption isotherms of (**c**) TiZSM-5 and (**d**) 4 wt% Ag/TiZSM-5; Fourier-transform infrared (FTIR) spectra of (**e**) TiZSM-5 and (**f**) 4 wt% Ag/TiZSM-5; and (**g**) zeta potentials of TiZSM-5, 4 wt% Ag/TiZSM-5, 4 wt% Ag/TiZSM-5/SHMP, and GIC containing 3% and 5% 4 wt% Ag/TiZSM-5/SHMP. SHMP: sodium hexametaphosphate; GIC: glass ionomer cement.

3.3. High-Resolution Transmission Electron Microscope (HRTEM)

Figure 5 presents high-resolution transmission electron microscopy (HR-TEM) images of the TiZSM-5 and fabricated 4 wt% Ag/TiZSM-5/SHMP/GIC composites. Figure 5a shows the morphology of the Ag/Ti-ZSM-5 zeolite with relatively well-dispersed, micron-sized crystals exhibiting distinct boundaries and limited agglomeration. These observations suggest that the overall crystal morphology was retained following silver impregnation. In contrast, the ZSM-5@Ag/Ti/SHMP/GIC composites shown in Figure 5b–d exhibit densely aggregated particles forming an interconnected composite network. Individual zeolite particles are less readily distinguishable and appear embedded within a continuous matrix, which is consistent with the embedding of the Ag/Ti-ZSM-5/SHMP particles within the glass ionomer cement (GIC) matrix. However, these images provide morphological features; interfacial interactions between the components, SHMP loading within the zeolite pores, and ion release cannot be determined from imaging alone.

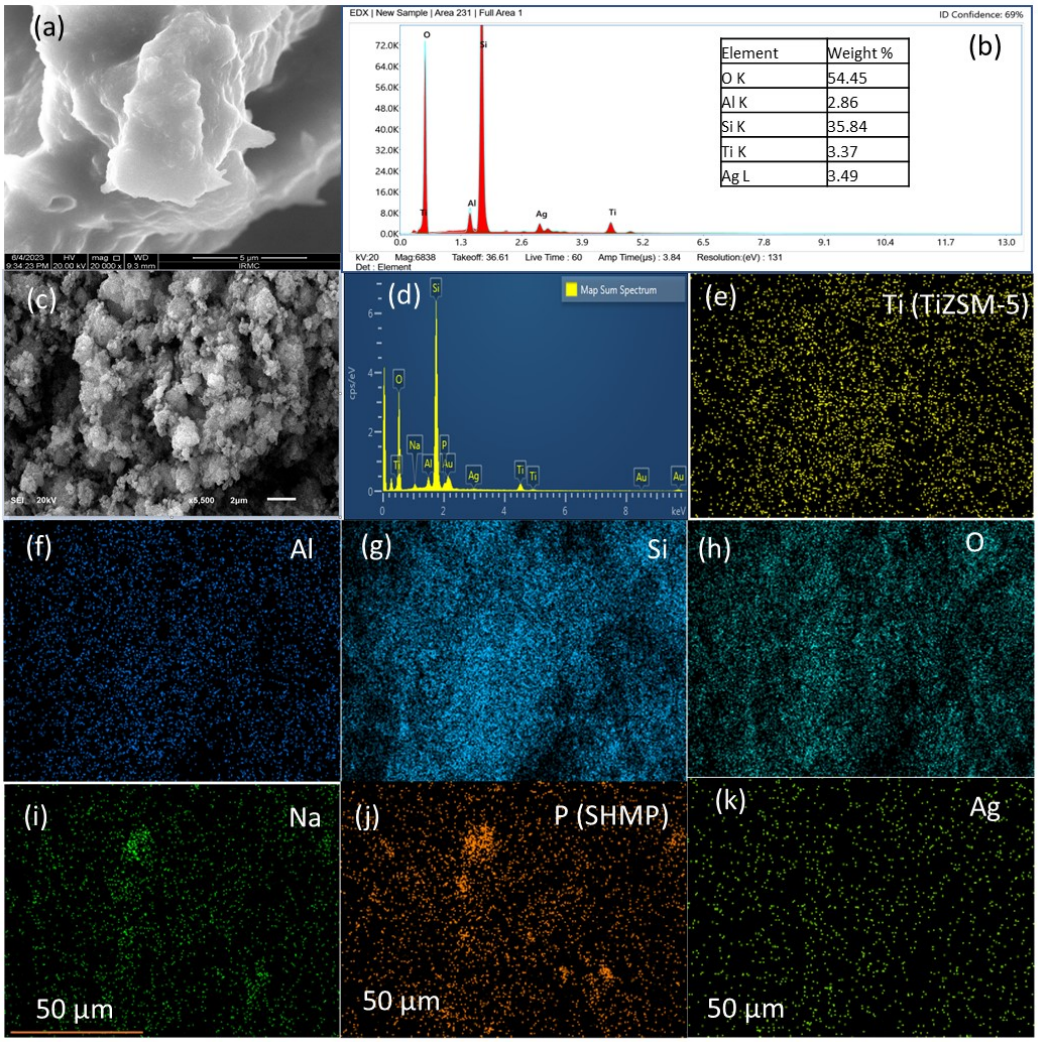


Figure 4. (**a**) SEM micrograph and (**b**) EDX spectrum of 4 wt% Ag/TiZSM-5; (**c**–**k**) SEM, EDX spectrum and micrograph of SHMP-functionalized 4 wt% Ag/TiZSM-5.

3.4. DRS-UV-Vis Spectroscopy, SHMP Release, Surface Roughness and Color Change

The UV-vis diffuse reflectance spectra of TiZSM-5 exhibit absorption features associated with oxygen-to-titanium charge-transfer transitions within the aluminosilicate matrix (Figure 6A). Bands at approximately 210–220 nm are commonly assigned to isolated tetrahedral Ti(IV), whereas absorption at 240–280 nm may involve higher-coordinate or extra-framework Ti species, including octahedral environments [28]. Following Ag impregnation, a slight decrease in absorption intensity suggests changes in the local optical environment, which is consistent with Ag–support interactions. Subsequent functionalization with SHMP largely preserves the spectral profile, suggesting no substantial alteration of the dominant Ti coordination environments. Together with the BET textural results, this observations are consistent with SHMP association with accessible surfaces and pores. Incorporating 5 wt% 4 wt% Ag/TiZSM-5 filler into glass ionomer cement (GIC) produces spectral differences relative to pristine GIC, which is consistent with the presence of the zeolite filler in the cement matrix.

The cumulative percentage release of SHMP was evaluated using a dialysis membrane technique. An initial burst release was observed, possibly reflecting the rapid release of loosely bound surface associated phosphate species. SHMP release exhibited an overall increase with time, reaching approximately 25% at 24 h, 27% at 48 h, and 33% at 72 h (Figure 6B). The continued increase between 24 and 72 h indicates prolonged release over

the experimental period. This behavior may reflect the gradual desorption and diffusion of phosphate species from the composite, although release kinetics require further analysis to establish the underlying mechanism. Related work by Hosida et al. (2019) [29] demonstrated hexametaphosphate release from modified glass ionomer cements with release influenced by concentration and particle size.

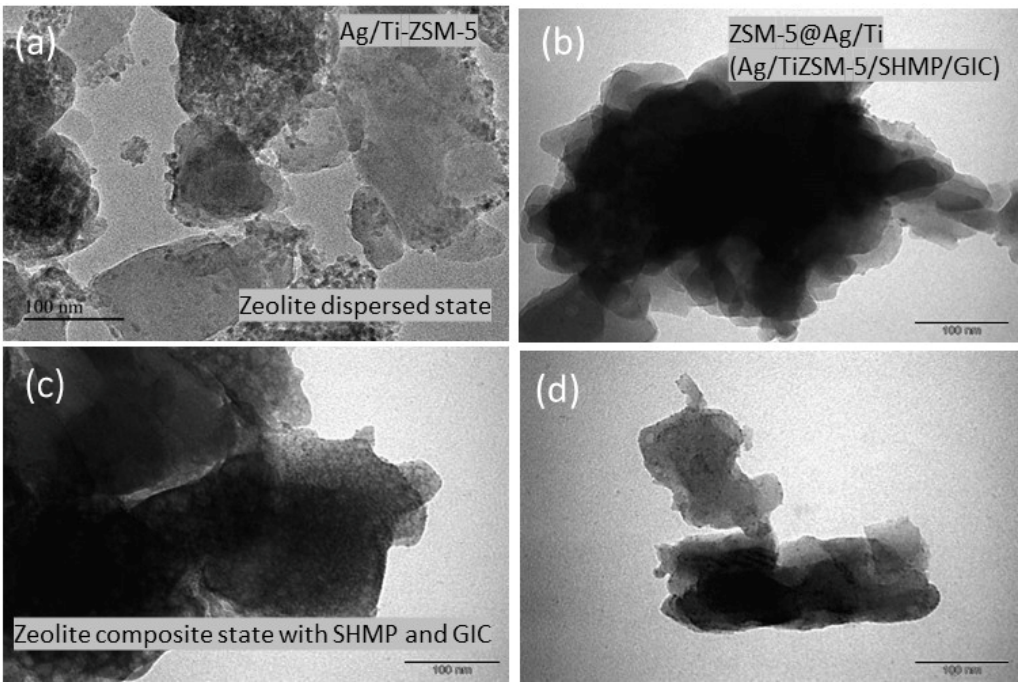


Figure 5. High-resolution transmission electron microscope images of (**a**) Ag/Ti-ZSM-5 and (**b**–**d**) Ag/Ti-ZSM-5/SHMP/GIC (ZSM-5@Ag/Ti).

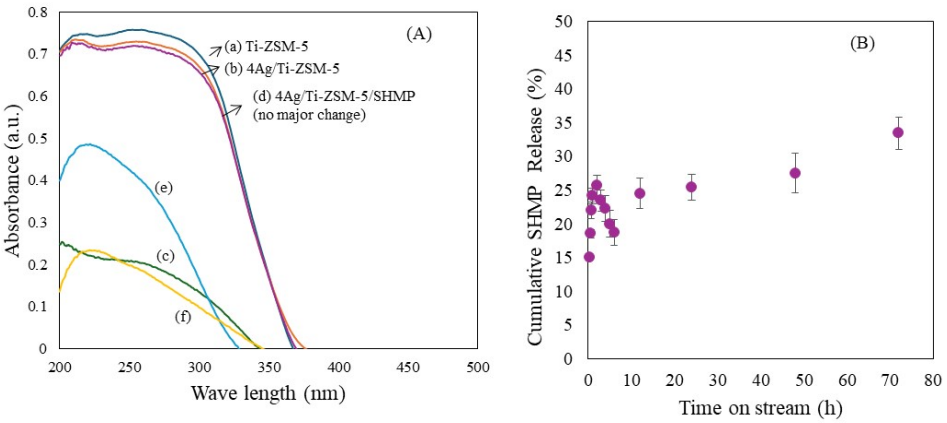


Figure 6. (**A**). Diffuse reflectance UV-visible spectra of (a) Ti-ZSM-5, (b) 4 wt% Ag/Ti-ZSM-5, (c) SHMP, (d) 4 wt% Ag/Ti-ZSM-5/SHMP, (e) GIC, (f) 4 wt% Ag/Ti-ZSM-5/SHMP/GIC. (**B**). Cumulative release (%) of sodium hexametaphosphate (SHMP) from 4 wt% Ag/TiZSM-5/SHMP over 72 h. Error bars represent the variability among replicate measurements.

Figure 7a shows the mean ± SD values for surface roughness. The data showed a significant difference among means ($F(6,28) = 4.08$, $p = 0.0046$, $\omega^2 = 0.35$, 95% CI 0.07–0.57). GIC with 3% Z-Sil@Ag had the highest Ra (0.89 ± 0.22 µm). This was significantly higher than the control (0.62 ± 0.10 µm, $p = 0.022$, 95% CI 0.027–0.509), 3% Z-Sil@Ag (0.68 ± 0.013 µm) and 1% Z-Sil@Ag (0.54 ± 0.05 µm, $p = 0.0015$, 95% CI 0.108–0.590) (Supplementary Table S1). No other groups differed significantly from the control or from each other ($p > 0.05$). These

results suggest that the ZSM-5@Ag/Ti group had surface roughness comparable to the control group, whereas Z-Sil@Ag–3% was the only group that differed significantly from the control; thus, roughness did not increase with concentration, as 5% dropped back to control levels.

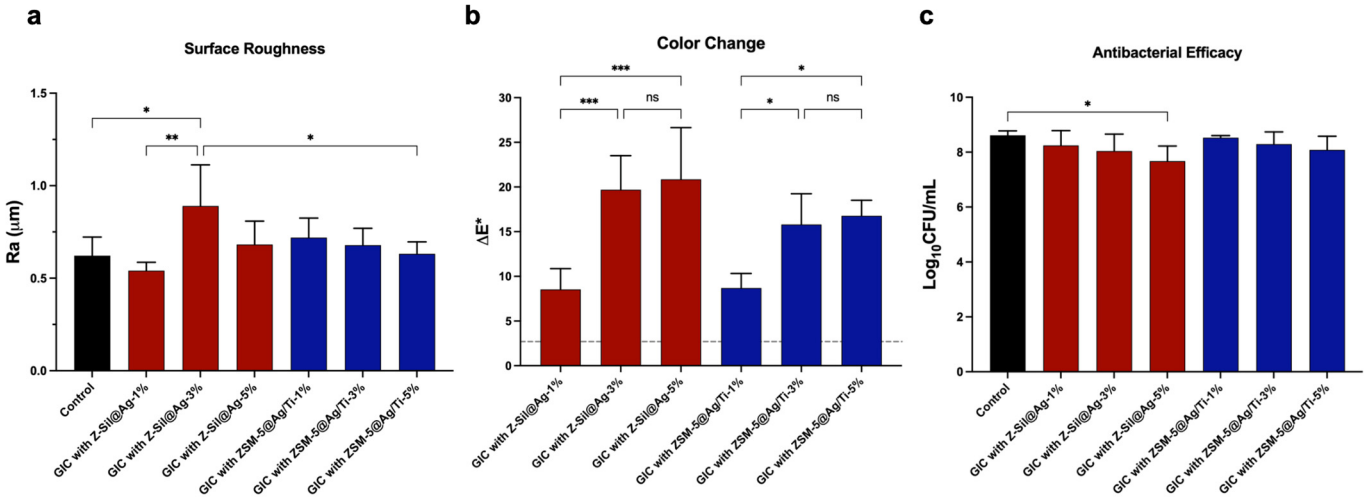


Figure 7. Surface roughness (Ra), color change (ΔE*), and antibacterial efficacy of GIC with Z-Sil@Ag and ZSM-5@Ag-Ti at 1, 3, and 5% compared with the control. (**a**) Surface roughness (Ra, μm) measured with a non-contact profilometer analyzed by one-way ANOVA with Tukey's multiple comparisons test. (**b**) Color change (ΔE*) of the studied groups relative to the control, analyzed by one-way ANOVA with Tukey's multiple comparisons test. The dashed line marks the 50:50% acceptability threshold (ΔE* = 2.7). All samples were above 2.7, which was analyzed by a one-sample *t*-test, $p < 0.01$. (**c**) Viable *Streptococcus mutans* counts (Log_{10} CFU/mL), analyzed by one-way ANOVA with Dunnett's multiple comparisons against the control. Values are presented as mean ± SD ($n = 5$) of the studied groups. * $p < 0.05$, ** $p < 0.01$, *** $p < 0.001$; ns, not significant.

For color change, the modified groups differed significantly ($F(5,24) = 11.97$, $p < 0.0001$, $\omega^2 = 0.65$, 95% CI 0.39–0.78). For both groups, 1% was significantly lower than at 3% and 5% (Z-Sil@Ag: 8.54 ± 2.32 vs. 19.70 ± 3.82 [CI = −17.88 to −4.43] and 20.86 ± 5.79, 95% CI −19.05 to −5.59, both $p < 0.001$; ZSM-5@Ag/Ti: 8.69 ± 1.63 vs 15.80 ± 3.44, 95% CI −13.99 to −0.05 and 16.79 ± 1.72, 95% CI −14.89 to −0.152, $p = 0.029$ and $p = 0.012$, respectively). In contrast, no significant difference was found between 3% and 5% for either group ($p > 0.99$), or between groups at the same concentration ($p > 0.44$), as shown in Figure 7b. Nevertheless, the mean ΔE values of all groups exceeded the commonly cited clinical acceptability threshold of 2.7 units [21].

3.5. Antibacterial Test

The antibacterial activity was evaluated against *S. mutans* on BHI agar in Figure 7c. It demonstrates that the most experimental groups did not differ significantly in their antibacterial activity ($F(6,28) = 2.41$, $p = 0.053$, $\omega^2 = 0.19$, 95% CI 0.00–0.46). However, the control group ((8.62 ± 0.16 $\log_{10}$ CFU/mL)) differed significantly from the Z-Sil@Ag–5% group (7.67 ± 0.55 log10 CFU/mL, $p = 0.015$, 95% CI 0.1517 to 1.732), indicating lower bacterial counts and thus higher antibacterial activity at the highest concentration. Although the remaining comparisons were not statistically significant, the ZSM-5@Ag/Ti groups showed slightly higher bacterial counts (8.53–8.09 $\log_{10}$ CFU/mL) than the Z-Sil@Ag groups (8.25–7.67 $\log_{10}$ CFU/mL). As lower CFU counts indicate greater antibacterial activity, this suggests a modest, non-significant trend toward a greater antibacterial effect of the Z-Sil@Ag formulations.

3.6. Microbial Adhesion Test

The adhesion rate of *Candida albicans* to the prepared discs was calculated and expressed in percentage. After the final incubation, the obtained viable colonies were counted. The cell counts of each disc demonstrated that the number of *C. albicans* that adhered to the disc was less than the number that had adhered to the control disc, as shown in Figure 8. All the synthesized discs tested had a potential effect on the adherence of *C. albicans* with adherence rates of 18%, 0.8%, 4% found with (B) ZSM-5@Ag/Ti 1%, (C) ZSM-5@Ag/Ti 3% and (D) ZSM-5@Ag/Ti 5%, respectively. Meanwhile, the adherence rate was found to be ~100%, 79%, and 13% with the discs (E) Z-Sil@Ag 1%, (F) Z-Sil@Ag 3% and (G) Z-Sil@Ag 5%, respectively. These adhesion data should be regarded as preliminary, as they were not confirmed by microscopy or biofilm biomass assays.

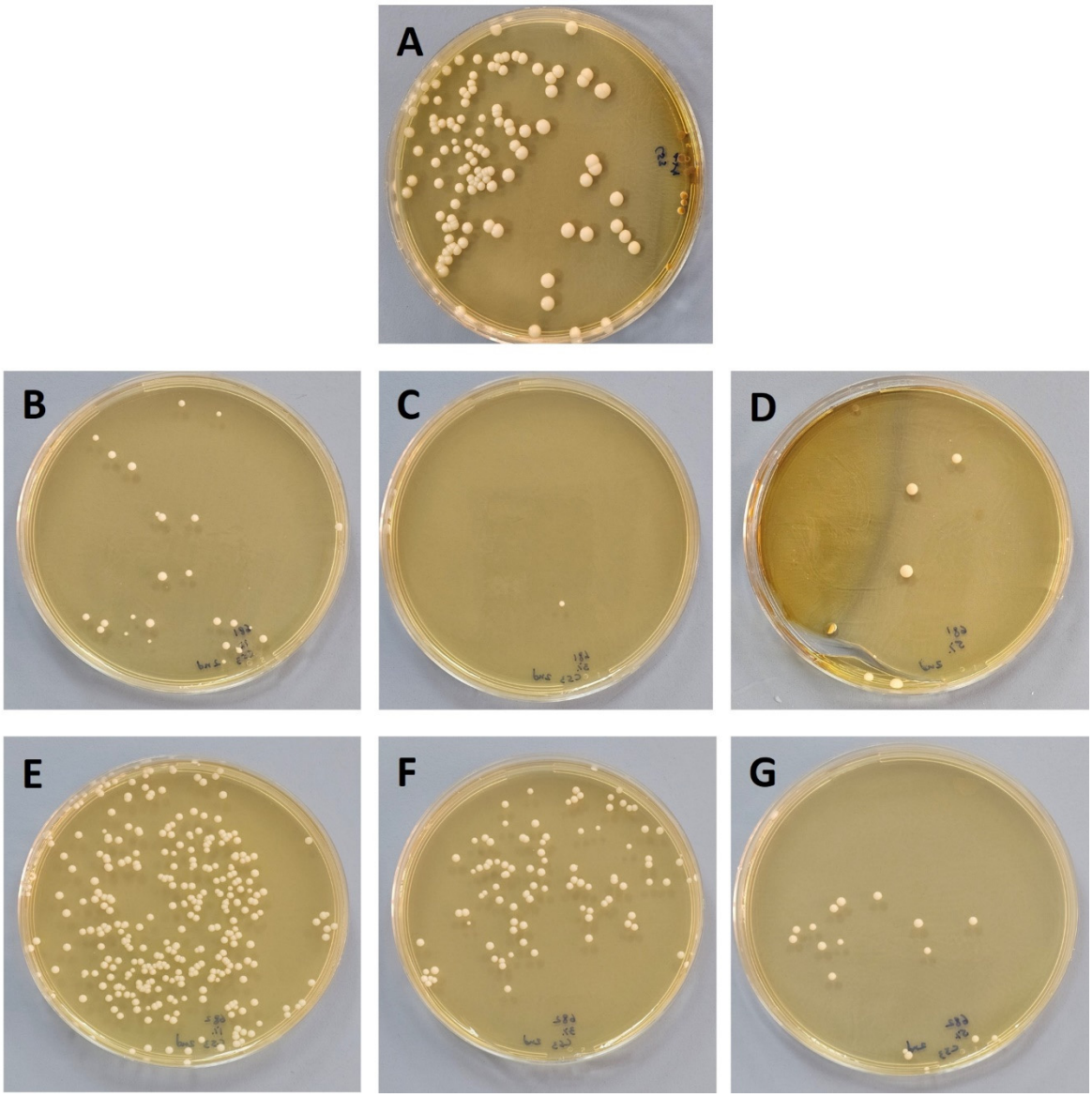


Figure 8. SDA plates depicting rate of adhesion of Candida on tested disc (**A**) GIC control, (**B**) ZSM-5@Ag/Ti 1%, (**C**) ZSM-5@Ag/Ti 3%, (**D**) ZSM-5@Ag/Ti 5%, (**E**) Z-Sil@Ag 1%, (**F**) Z-Sil@Ag 3%, (**G**) Z-Sil@Ag 5%.

3.7. In Vitro Cytotoxicity

The cytotoxicity of the tested 4 wt% Ag/Ti-ZSM-5 composites was evaluated in human foreskin fibroblasts (HFF-1) using the MTT assay after 48 h of exposure to six concentrations ranging from 6.25 to 200 µg/mL (Figure 9). Free $AgNO_3$ exhibited marked, dose-dependent cytotoxicity with an IC_{50} of 3 µg/mL. In contrast, all 4 wt% Ag/Ti-ZSM-5 composites-maintained cell viability above 80% throughout the tested concentration range. For 4 wt% Ag/Ti-ZSM-5, cell viability decreased by 10% from the highest to the lowest concentration. Although this difference was statistically significant ($p < 0.01$), viability remained within the non-cytotoxic range. Ti-ZSM-5 alone showed a slight decrease in viability, reaching 73% at the highest concentration with no statistically significant differences across concentrations. Interestingly, adding SHMP enhanced the biocompatibility of 4 wt% Ag/Ti-ZSM-5/SHMP, as cells remained 100% viable at all tested concentrations, with no significant differences among concentrations. Similarly, 4 wt% Ag/Ti-ZSM-5/SHMP/GIC, which contains 1% 4 wt% Ag/TiZ5/SHMP, maintained a viability of approximately 86–94% with no significant change across the concentration range. These values were close to those for GIC alone (84–97%).

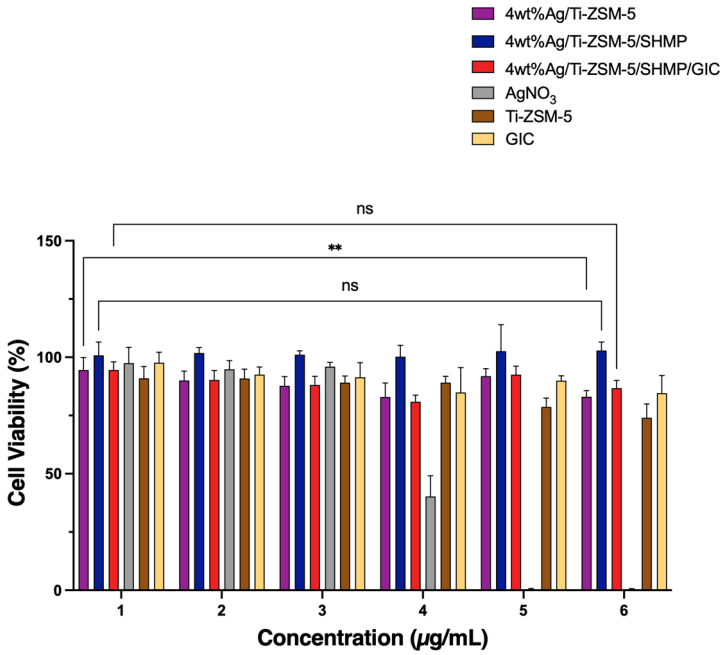


Figure 9. In vitro cytotoxicity of tested composites by MTT assay. HFF-1 cells were treated for 48 h with six concentrations of 4 wt% Ag/Ti-ZSM-5, 4 wt% Ag/Ti-ZSM-5/SHMP, 4 wt% Ag/Ti-ZSM-5/SHMP/GIC, and the controls $AgNO_3$, Ti-ZSM-5, and GIC. Viability was expressed as a percentage of untreated control cells. For clarity, only comparisons between the lowest and highest concentrations within each composite group are shown. Of these, only 4 wt% Ag/Ti-ZSM-5 showed a significant decrease (** $p < 0.01$). Most other comparisons of the main Ag-loaded composites were not significant (ns). Data are presented as mean ± SD ($n = 2$).

Notably, the half-maximal inhibitory concentration (IC_{50}) could not be determined for 4 wt% Ag/Ti-ZSM-5, 4 wt% Ag/Ti-ZSM-5/SHMP, 4 wt% Ag/Ti-ZSM-5/SHMP/GIC, Ti-ZSM-5, and GIC because cell viability remained above 80% at all tested concentrations. Therefore, their IC_{50} values were estimated to exceed 200 µg/mL, which was the highest concentration tested. These findings indicate that the composites are non-cytotoxic to HFF-1 cells within the tested range.

4. Discussion

This in vitro study aimed to develop a novel impregnation technique for SHMP to 4 wt% Ag impregnated on microporous TiZSM-5 zeolite. XRD showed that the MFI framework of TiZSM-5 was preserved after silver impregnation, and the deposition of SHMP on the zeolite particles was supported by SEM and EDX elemental mapping. The functionalization process was planned to enhance the antibacterial effect of GIC and increase the physical properties of the proposed material. The surface analysis of 4 wt% Ag impregnated on TiZSM-5 found that phosphate, and sodium were present in EDX, and SEM images showed salt deposits on the surface of the particles.

The SHMP-functionalized 4 wt% Ag/TiZSM-5 zeolite showed preliminary results that may be of interest for restorative materials. The nature of SHMP is poorly discussed in the literature when combined with restorative materials; however, it has shown a liquifying property, and the properties could be subsequently affected. It was hypothesized that a porous carrier such as zeolite could store SHMP and release it gradually, thereby limiting its adverse effect on the GIC matrix. In this context, Ge et al. found that silver-loaded zeolite has a similar surface morphology to GIC [30,31].

To the best of our knowledge, no previous studies have evaluated the surface roughness or color change in GIC-modified with SHMP-functionalized TiZSM-5 zeolite particles. In the present study, incorporating ZSM-5@Ag/Ti did not significantly alter the surface roughness compared with the control. In contrast, a previous study reported that incorporating Ag-Zn zeolite into acrylic resin at concentrations of 0.50% and 0.75% reduced surface roughness compared to the control group [32]. This might be related to the evaporation of the monomer during the curing process may have caused the cure acrylic resin to develop numerous porosities and voids, which filled with the Ag-Zn zeolite material and produced surfaces that were smoother than those of the control group. The majority of the porosities and gaps in the resin matrix were filled by Ag-Zn zeolite, creating a smoother surface [32].

GIC is widely used for luting or esthetic restoration for people of all ages [1,2]. Therefore, the effects of additives on its color and shape requires careful consideration. For color change, the analysis revealed that the majority of the groups showed no statistically significant differences. The ZSM-5@Ag/Ti–5% group exhibited the lowest mean color change. The interaction between the particles and the luting GIC matrix, which can modify light scattering, translucency, and overall color perception, may be connected to the observed color. However, the lack of statistically significant changes between the majority of the experimental groups may be due to the effect of the silver or titanium, which may affect the color stability of GIC under the examined conditions. However, all groups exceeded the commonly cited clinical acceptability threshold of about 3.3 ΔE units, including the best-performing group.

This finding is clinically relevant because color differences above this threshold are likely to be perceptible and may limit the use of these formulations in esthetically demanding areas. Silver-containing materials are prone to discoloration [13], and this should be considered when such additives are used in tooth-colored materials. Therefore, the modified formulations may be more suitable for applications where esthetics is less critical, such as luting, liners and bases, or posterior and root-surface restorations in high-caries-risk patients. Future studies should evaluate lower filler concentrations (e.g., below 1 wt%), more color-stable silver species or alternative antimicrobial ions, and the addition of opacifying or color-masking agents, as well as color stability after aging. A previous study conducted randomized clinical research that assessed the use of bleaching gel containing 1% SHMP and found that it decreased bleaching sensitivity without negatively impacting the efficacy of at-home bleaching [33]. The results of that study support the potential dental applications and biocompatibility of SHMP-containing formulations, even though it examined SHMP in

the context of tooth bleaching rather than as a zeolite composite integrated with GIC. As a result, adding SHMP-based zeolite to dental materials could be a promising strategy as long as their concentration is carefully regulated to maintain the material's functional and esthetic qualities.

Zeolites have been shown in earlier studies to be biocompatible and nontoxic [22,31]; therefore, the cytotoxicity of the present formulations was evaluated against a normal cell line (HFF-1) to further confirm their biocompatibility. Two types of microbial testing were conducted to ensure the potency of proposed theory. For antibacterial activity, *S. mutans* was chosen because it is one of the principal cariogenic bacteria in the oral cavity. The silver- and silver/titanium-containing groups did not differ significantly from the control in their antibacterial activity against *S. mutans*, except for the Z-Sil@Ag–5% group, which showed significantly lower bacterial counts. This is consistent with the known antibacterial effect of silver against *S. mutans* [34]. The growth inhibition was comparable to that observed by Loyola-Rodriguez et al., who discovered an effective *S. mutans* growth suppression in comparison to various bacterial species [4]. Hosida et al. found that when SHMP was used in low concentrations, it had an effect on bacterial colonies; however, as the concentration increases, the antibacterial effect along with fluoride increases [35]. Ge KX et al. tested the bacterial growth and kinetic properties and found that groups with silver zeolite had less bacterial growth over a 7-day period compared with the control [30]. Surface-attached bacteria had more dead cells upon immunofluorescence imaging compared to the control [30]. It is well established that after being exposed to sucrose, *S. mutans* produced lactic acid, which lowered pH and may have contributed to the development of carious lesions in clinical settings [36]. Previous studies tested SHMP biofilm and found out that pH was significantly impacted by the application of HMP solutions, and HMP was found to raise pH levels both before and following sucrose exposure [35,37]. It may therefore be hypothesized that if SHMP is released from the composite, it could bind H+ and act as a buffering agent; however, neither SHMP release nor pH was measured in the present study. In regard to fungal adhesion, the ZSM-5@Ag/Ti groups showed lower *C. albicans* adhesion than the Z-Sil@Ag groups, with the lowest adherence in the ZSM-5@Ag/Ti 3% group (0.8%), whereas the Z-Sil@Ag 1% group showed adhesion similar to that of the control (~100%). Differences in cell wall and membrane structure may explain why *C. albicans* appeared more susceptible than *S. mutans* in the present study [38–40]; however, this explanation remains speculative, as the two assays used different methodologies and their results are not directly comparable. The antibacterial activity of the nanoparticles themselves is dependent on the charge of the particles' external surface, which is regulated by the stabilizers and capping agents used in the synthesis; as a result, the produced silver NP can be regarded as negatively charged [39,40]. The mechanism of silver NP action is dependent on the bacterial membranes' outer charge, which could account for *S. mutans'* reduced susceptibility. Additionally, the silver NP's chemical and physical characteristics in relation to the release of Ag+ ions are significant [40].

In this study, the integration of Ag-impregnated TiZSM-5 with SHMP, followed by incorporation into the GIC matrix, has been characterized using different physicochemical techniques. The aluminosilicate zeolite provides a structurally robust support for silver species. XRD identifies the zeolitic MFI phase along with metallic Ag (Figure 3a,b), while BET and FT-IR confirm the systemic pore interactive deposition of silver with hydroxyl groups of titanium-incorporated zeolite (Figure 3c–f). The zeta potential reveals a significant improvement in the electrostatic stabilization with SHMP addition to ZSM-5@Ag/Ti (Figure 3g). SEM-EDX and HRTEM findings confirm the elemental composition and support changes in pore accessibility (Figures 4 and 5). The largely retained DRS UV-visible absorption features after SHMP functionalization suggest no major changes in the optically

detectable Ti- and Ag-related species. SHMP may associate with accessible zeolite surfaces and pore entrances through phosphate-mediated interactions. The accompanying change in zeta potential supports the modification of the interfacial charge; improved colloidal stability should be inferred only if the magnitude of the zeta potential increases sufficiently under comparable measurement conditions. The overall increase in SHMP release with time suggests a gradual liberation of phosphate-containing species from the composite, potentially through desorption and diffusion (Figure 6A,B). Incorporation into GIC may further influence the water penetration and transport of released species. The resulting restorations generally maintained surface roughness comparable to the control. Reduced Candida albicans adhesion, particularly for the 3% formulation, indicates an anti-adhesion effect under the tested conditions, whereas the absence of significant improvement against Streptococcus mutans limits claims of broad antimicrobial activity. Although the 5% formulation exhibited the lowest mean color change, all groups exceeded the stated clinical acceptability threshold ($\Delta E > 3.3$), indicating that color stability requires improvement (Figures 7 and 8). Long-term Ag-ion release studies are needed to determine whether silver availability contributes to the observed biological effects and whether antimicrobial activity persists over time.

Finally, examining the structural, physical and antimicrobial impact of the particles on GIC, the results of this study suggest that the SHMP-functionalized biocompatible Ag/Ti-ZSM-5 composite can be incorporated into GIC without significantly affecting surface roughness and may reduce *C. albicans* adhesion. However, no significant improvement in antibacterial activity against *S. mutans* was observed. Further studies with longer exposure periods are required to characterize Ag release from the microporous Ti-ZSM-5 matrix and establish antibacterial action for its potential contribution to caries control. In addition, it is also necessary to test important properties, including setting time, mechanical strength, and fluoride release after conducting an aging test to simulate oral conditions.

5. Conclusions

This study developed a micron-sized, SHMP-functionalized 4 wt% Ag/Ti-ZSM-5 composite for application in GIC-based dental restorations aimed at reducing microbial adhesion while maintaining comparable surface roughness. Characterization using XRD, BET, FT-IR, zeta potential, SEM–EDX, HRTEM, and DRS UV-visible spectroscopy supported the retention of the MFI structure, silver impregnation, and changes in surface properties following the integration of SHMP.

GIC formulations containing Ag/Ti-ZSM-5/SHMP into GIC exhibited surface roughness generally comparable to the unmodified GIC. Color change was lower at 1% than at 3% and 5% additive concentrations; however, all groups exceeded the clinical acceptability threshold for color change ($\Delta E > 2.7$), which may limit their use in esthetic areas. Ag/Ti-ZSM-5 composites maintained HFF-1 cell viability above 80% throughout the tested concentration range, indicating favorable in vitro cytocompatibility under the experimental conditions. The antibacterial activity of ZSM-5@Ag/Ti formulations against *Streptococcus mutans* did not differ significantly from that of the control, whereas preliminary adhesion assays suggested reduced *Candida albicans* adhesion. Overall, these findings demonstrate the feasibility of incorporating SHMP-functionalized Ag/Ti-ZSM-5 into GIC with a sustained release of SHMP. Further studies are required to evaluate long-term silver release, mechanical and setting properties, fluoride release, color stability after aging, remineralization potential, and in vivo performance before clinical application.

Supplementary Materials: The following supporting information can be downloaded at: https://www.mdpi.com/article/10.3390/dj14110749/s1, Table S1: Descriptive statistics of the tested properties (surface roughness, color changes ΔE* and antibacterial test).

Author Contributions: Conceptualization, R.J.B.; methodology, A.A.A., T.A., F.M.A., N.A., R.A., R.J.B., S.A., and S.R.; software, T.A., and S.A.; validation, R.J.B., S.A. and R.A.; formal analysis, T.A. and S.A.; investigation, R.J.B., A.A.A., T.A., F.M.A., N.A., R.A., S.A. and S.R.; resources, R.J.B. and A.A.A.; data curation, A.A.A., T.A., F.M.A. and N.A.; writing—original draft preparation, R.J.B., A.A.A., T.A., F.M.A., N.A., R.A., S.A. and S.R.; writing—review and editing, R.J.B. and F.M.A.; visualization, R.J.B.; supervision, R.J.B., R.A.; project administration, R.J.B.; funding acquisition, R.J.B., All authors have read and agreed to the published version of the manuscript.

Funding: The author Rabindran Jermy Balasamy would like to acknowledge that the research grant was funded by the Research, Development, and Innovation Authority (RDIA), Kingdom of Saudi Arabia, Reactivating & Rebuilding of Existing Labs Initiative with grant number (12968-iau-2023-iau-R-3-1-HW-).

Institutional Review Board Statement: Not applicable. This study used commercially available, established cell lines with the corresponding ATCC accession numbers provided in the Materials and Methods section. No human participants or animal experiments were involved.

Informed Consent Statement: Not Applicable.

Data Availability Statement: Supporting data are provided in the Supplementary Materials. Additional data are available from the corresponding author upon reasonable request.

Acknowledgments: During the preparation of this manuscript, the authors used ChatGPT-6.1 (OpenAI, San Francisco, CA, USA; https://chatgpt.com, accessed 1 November 2026) for generating and refining the graphical abstract. The authors reviewed and edited the output and take full responsibility for the content of this publication. The authors acknowledge the technical assistance of Jonal Colendres and Victonette Acson.

Conflicts of Interest: The authors declare no conflicts.

References

1. Tonprasong, W.; Inokoshi, M.; Shimizubata, M.; Yamamoto, M.; Hatano, K.; Minakuchi, S. Impact of direct restorative dental materials on surface root caries treatment. Evidence based and current materials development: A systematic review. *Jpn. Dent. Sci. Rev.* **2022**, *58*, 13–30. [CrossRef]
2. Lohbauer, U. Dental glass ionomer cements as permanent filling materials?—Properties, limitations future trends. *Materials* **2009**, *3*, 76–96. [CrossRef]
3. Sidhu, S.K.; Nicholson, J.W. A review of glass-ionomer cements for clinical dentistry. *J. Funct. Biomater.* **2016**, *7*, 16. [CrossRef]
4. Loyola-Rodriguez, J.P.; Garcia-Godoy, F.; Lindquist, R. Growth inhibition of glass ionomer cements on mutants streptococci. *Pediatr. Dent.* **1994**, *16*, 346. [PubMed]
5. Hafshejani, T.M.; Zamanian, A.; Venugopal, J.R.; Rezvani, Z.; Sefat, F.; Saeb, M.R.; Vahabi, H.; Zarrintaj, P.; Mozafari, M. Antibacterial glass-ionomer cement restorative materials: A critical review on the current status of extended-release formulations. *J. Control. Release* **2017**, *262*, 317–328. [CrossRef]
6. Baehni, P.C.; Takeuchi, Y. Anti-plaque agents in the prevention of biofilm-associated oral diseases. *Oral Dis.* **2003**, *9*, 23–29. [CrossRef]
7. Mallineni, S.K.; Sakhamuri, S.; Kotha, S.L.; AlAsmari, A.R.G.M.; AlJefri, G.H.; Almotawah, F.N.; Mallineni, S.; Sajja, R. Silver Nanoparticles in Dental Applications: A Descriptive Review. *Bioengineering* **2023**, *10*, 327. [CrossRef] [PubMed] [PubMed Central]
8. Abed, F.M.; Kotha, S.B.; AlShukairi, H.; Almotawah, F.N.; Alabdulaly, R.A.; Mallineni, S.K. Effect of Different Concentrations of Silver Nanoparticles on the Quality of the Chemical Bond of Glass Ionomer Cement Dentine in Primary Teeth. *Front Bioeng. Biotechnol.* **2022**, *10*, 816652. [CrossRef] [PubMed] [PubMed Central]
9. Dionísio, T.; Brandão, P.; Machado, V.; Botelho, J.; Mendes, J.J.; Fonte, P. Recent advances in antibacterial nanoformulations for endodontic applications. *Expert Opin. Drug Deliv.* **2025**, *22*, 1117–1136. [CrossRef] [PubMed]

10. Qing, Y.; Cheng, L.; Li, R.; Liu, G.; Zhang, Y.; Tang, X.; Wang, J.; Liu, H.; Qin, Y. Potential antibacterial mechanism of silver nanoparticles and the optimization of orthopedic implants by advanced modification technologies. *Int. J. Nanomed.* **2018**, *13*, 3311–3327. [CrossRef] [PubMed] [PubMed Central]
11. Kanani, H.; Khubchandani, M. Comparative Evaluation of Mechanical Properties and Bond Strength of Glass Ionomer Cement reinforced with three different concentrations of Silver Nanoparticles as against Conventional Glass Ionomer Cement in Primary Teeth. *F1000Res* **2024**, *12*, 1084. [CrossRef] [PubMed] [PubMed Central]
12. Bruna, T.; Maldonado-Bravo, F.; Jara, P.; Caro, N. Silver Nanoparticles and Their Antibacterial Applications. *Int. J. Mol. Sci.* **2021**, *22*, 7202. [CrossRef]
13. Guo, T.; Wang, D.; Gao, S.S. Incorporating nanosilver with glass ionomer cement-A literature review. *J. Dent.* **2024**, *149*, 105288. [CrossRef]
14. Hook, E.R.; Owen, O.J.; Bellis, C.A.; Holder, J.A.; O'Sullivan, D.J.; Barbour, M.E. Development of a novel antimicrobial-releasing glass ionomer cement functionalized with chlorhexidine hexametaphosphate nanoparticles. *J. Nanobiotechnol.* **2014**, *12*, 3. [CrossRef]
15. Choi, Y.; Sun, W.; Kim, Y.; Kim, I.R.; Gong, M.K.; Yoon, S.Y.; Bae, M.K.; Park, B.S.; Park, S.B.; Kim, Y.I. Effects of Zn-doped mesoporous bioactive glass nanoparticles in etch-and-rinse adhesive on the microtensile bond strength. *Nanomaterials* **2020**, *10*, 1943. [CrossRef]
16. Akram, Z.; Aati, S.; Ngo, H.; Fawzy, A. PH-dependent delivery of chlorhexidine from PGA grafted mesoporous silica nanoparticles at resin-dentin interface. *J. Nanobiotechnol.* **2021**, *19*, 43. [CrossRef]
17. Morankar, D.; Barhate, K.; Hatvate, N. ZSM-5 zeolite: Structural features, catalytic properties, and multidisciplinary applications in organic synthesis, material science, and environmental remediation. *Coord. Chem. Rev.* **2026**, *549*, 217245. [CrossRef]
18. Tan, J.; Hao, J.; Vann, D.; Pavelić, K.; Ozer, F. Effect of zeolite incorporation on the ion release properties of silver-reinforced glass ionomer cement. *Biomimetics* **2024**, *9*, 365. [CrossRef]
19. Ibrahim, M.S.; Alatiyyah, F.M.; Mohammed, K.A.; Alhawaj, H.N.; Balhaddad, A.A.; Ibrahim, A.S. The Effect of Salbutamol and Budesonide Pediatric Doses on Dental Enamel and Packable and Flowable Composites: Microhardness, Surface Roughness and Color. *Pharmaceutics* **2023**, *15*, 2527. [CrossRef]
20. Ba-Armah, I.; Alenizy, M.; Almutairi, N.; Alqarni, H.; Alhussein, A.; Masri, R.; Hack, G.D.; Oates, T.W.; Sun, J.; Weir, M.D.; et al. Novel Antibacterial Resin Coating for Dental Provisional Crowns to Suppress Biofilms and Inhibit Secondary Caries. *Coatings* **2024**, *14*, 1370. [CrossRef]
21. Paravina, R.D.; Ghinea, R.; Herrera, L.J.; Bona, A.D.; Igiel, C.; Linninger, M.; Sakai, M.; Takahashi, H.; Tashkandi, E.; Perez; et al. Color difference thresholds in dentistry. *J. Esthet. Restor. Dent.* **2015**, *27*, S1–S9. [CrossRef]
22. Okada, K. Is omega squared less biased? A comparison of three major effect size indices in one-way ANOVA. *Behaviormetrika* **2013**, *40*, 129–147. [CrossRef]
23. Rostami-Vartooni, A.; Moradi-Saadatmand, A. Green synthesis of magnetically recoverable Fe_3O_4/HZSM-5 and its Ag nanocomposite using *Juglans regia* L. leaf extract and their evaluation as catalysts for reduction of organic pollutants. *IET Nanobiotechnol.* **2019**, *13*, 407–415. [CrossRef]
24. Fu, Z.; Pan, Y.; Wang, R.; Suo, S.; Wang, Z.; Peng, X.; Fang, P. The Use of Metal/ZSM-5 Nanosheet for Efficient Catalytic Cracking of Cross-Linked Polyethylene for High-Voltage Cable Insulation. *Materials* **2025**, *18*, 4675. [CrossRef]
25. Rashidvand, A.; Kheirmand, M.; Roozbehani, B.; Hosseini, S.H. Fabrication and characterization of ZSM-5 zeolite modified with silver and assessing its performance in petroleum waste cracking process. *Arab. J. Chem.* **2023**, *16*, 105330. [CrossRef]
26. Qi, Y.; Yang, H.; Li, C.; Li, H. Enhanced adsorption of trace ethylene on Ag/NZ5 modified with ammonia: Hierarchical structure and metal dispersion effects. *Molecules* **2024**, *29*, 981. [CrossRef]
27. Mei, Y.; Chen, W.; Chen, X. The effect of sodium hexametaphosphate on the dispersion and polishing performance of lanthanum–cerium-based slurry. *Materials* **2024**, *17*, 4901. [CrossRef]
28. Zhang, T.; Zuo, Y.; Liu, M.; Song, C.; Guo, X. Synthesis of Titanium Silicalite-1 with High Catalytic Performance for 1-Butene Epoxidation by Eliminating the Extraframework Ti. *ACS Omega* **2016**, *1*, 1034–1040. [CrossRef]
29. Hosida, T.Y.; Delbem, A.C.B.; Morais, L.A.; Moraes, J.C.S.; Duque, C.; Souza, J.A.S.; Pedrini, D. Ion release, antimicrobial and physio-mechanical properties of glass ionomer cement containing micro or nanosized hexametaphosphate, and their effect on enamel demineralization. *Clin. Oral Investig.* **2019**, *23*, 2345–2354. [CrossRef]
30. Ge, K.X.; Lung, C.Y.; Lam, W.Y.; Chu, C.H.; Yu, O.Y. A novel glass ionomer cement with silver zeolite for restorative dentistry. *J. Dent.* **2023**, *133*, 104524. [CrossRef]
31. Samiei, M.; Ghasemi, N.; Asl-Aminabadi, N.; Divband, B.; Golparvar-Dashti, Y.; Shirazi, S. Zeolite-silver-zinc nanoparticles: Biocompatibility and their effect on the compressive strength of mineral trioxide aggregate. *J. Clin. Exp. Dent.* **2017**, *9*, 356–360. [CrossRef]
32. Aljafery, A.M.; Al-Jubouri, O.M.; Wally, Z.J.; Almusawi, R.M.; Abdulrudha, N.H.; Haider, J. The Effects of Incorporating Ag-Zn Zeolite on the Surface Roughness and Hardness of Heat and Cold Cure Acrylic Resins. *J. Compos. Sci.* **2022**, *6*, 85. [CrossRef]

33. Mohammadipour, H.S.; Bagheri, H.; Akbari, M.; Behzadi, S.; Ramezanian, N.; Javanshir, S.J.; Khorshid, M. The effect of sodium hexametaphosphate on sensitivity and whitening effectiveness of an at-home bleaching gel: A randomized, triple-blinded clinical trial. *Quintessence Int.* **2021**, *52*, 596–605. [CrossRef]
34. Besinis, A.; De Peralta, T.; Handy, R.D. The antibacterial effects of silver, titanium dioxide and silica dioxide nanoparticles compared to the dental disinfectant chlorhexidine on Streptococcus mutans using a suite of bioassays. *Nanotoxicology* **2014**, *8*, 742935. [CrossRef]
35. Hosida, T.Y.; Pessan, J.P.; Cavazana, T.P.; Sampaio, C.; de Morais, L.A.; Monteiro, D.R.; Delbem, A.C. Effects of Sodium Hexametaphosphate and Fluoride on the pH and Inorganic Components of Streptococcus mutans and Candida albicans Biofilm after Sucrose Exposure. *Antibiotics* **2022**, *11*, 1044. [CrossRef]
36. Pitts, N.B.; Zero, D.T.; Marsh, P.D.; Ekstrand, K.; Weintraub, J.A.; Ramos-Gomez, F.; Tagami, J.; Twetman, S.; Tsakos, G.; Ismail, A. Dental Caries. *Nat. Rev. Dis. Primers* **2017**, *3*, 17030. [CrossRef]
37. Cavazana, T.P.; Pessan, J.P.; Hosida, T.Y.; Monteiro, D.R.; Delbem, A.C.B. PH changes of mixed biofilms of Streptococcus mutans and Candida albicans after exposure to sucrose solutions in vitro. *Arch. Oral Biol.* **2018**, *90*, 9–12. [CrossRef]
38. Malanovic, N.; Lohner, K. Gram-positive bacterial cell envelopes: The impact on the activity of antimicrobial peptides. *Biochim. Biophys. Acta* **2016**, *1858*, 936–946. [CrossRef]
39. Mendes-Gouvêa, C.C.; do Amaral, J.G.; Fernandes, F.A.; Fernandes, G.L.; Gorup, L.F.; Camargo, E.R.; Delbem, A.C.B.; Barbosa, D.B. Sodium trimetaphosphate and hexametaphosphate impregnated with silver nanoparticles: Characteristics and antimicrobial efficacy. *Biofouling* **2018**, *34*, 299–308. [CrossRef]
40. Abbaszadegan, A.; Ghahramani, Y.; Gholami, A.; Hemmateenejad, B.; Dorostkar, S.; Nabavizadeh, M.; Sharghi, H. The effect of charge at the surface of silver nanoparticles on antimicrobial activity against gram-positive and gram-negative bacteria: A preliminary study. *J. Nanomater.* **2015**, *2015*, 720654. [CrossRef]

Disclaimer/Publisher's Note: The statements, opinions and data contained in all publications are solely those of the individual author(s) and contributor(s) and not of MDPI and/or the editor(s). MDPI and/or the editor(s) disclaim responsibility for any injury to people or property resulting from any ideas, methods, instructions or products referred to in the content.